Chinese Journal of
POLYMER SCIENCE

RESEARCH ARTICLE

https://doi.org/10.1007/s10118-026-3605-x
Chinese J. Polym. Sci. **2026**, *44*, 2305–2321

Chain Rigidity as a Key Regulator on Grafting Density and Dispersity of Polymer Brushes: Insights from Coarse-Grained Molecular Dynamics Simulations

Zheng-Jie Zhang[a,†], Wei-Shao Xu[d,†], Li-Jun Ma[b], Ying-Xiang Li[a], Yu-Qi Guo[f], Guo-Jie Zhang[e], Zhong-Yan Zhang[c*], Yan Wang[a*], and Hong Liu[a*]

[a] *Key Laboratory of Theoretical Chemistry of Environment Ministry of Education, School of Environment, South China Normal University, Guangzhou 510006, China*
[b] *School of Chemistry, South China Normal University, Guangzhou 510006, China*
[c] *Institute of Systems and Physical Biology, Shenzhen Bay Laboratory, Shenzhen 518132, China*
[d] *Dongguan HEC Tech R & D Co., Ltd., Dongguan 523871, China*
[e] *Department of Chemical Engineering, School of Chemistry and Chemical Engineering, Guangzhou University, Guangzhou 510006, China*
[f] *Department of Chemical and Material Engineering, Lyuliang University, Lvliang 033001, China*

Electronic Supplementary Information

Abstract Polymer brush-based surface modification plays a crucial role in tailoring material properties across a wide range of applications, from biomedicine to electronics. Grafting density and dispersity are key parameters governing the performance of polymer brushes; however, the influence of polymer chain rigidity on these characteristics remains insufficiently understood. Polymer chain rigidity is intrinsically determined by chemical structure and can be further modulated by intramolecular and intermolecular interactions, solvent quality, external fields, and topological constraints. In this work, we focus on isolating the role of chain rigidity by controlling it through intramolecular bond-angle interactions in coarse-grained molecular dynamics simulations with an implicit solvent description, allowing a systematic investigation of its role in polymer brush fabrication *via* both "grafting-to" and "grafting-from" strategies using a stochastic reaction model. For the grafting-to strategy, a moderate increase in chain rigidity enhances grafting density, whereas excessive rigidity restricts chain mobility, thereby hindering grafting efficiency. We further examine the effects of polymer chain length, solution concentration, and surface grafting site density, revealing that grafting kinetics are governed by the cooperative interplay of these factors. To optimize grafting density in binary polymer brushes of flexible and rigid chains using the "grafting-to" strategy, we compare three grafting approaches—flexible-first/rigid-second (F/R), rigid-first/flexible-second (R/F), and simultaneous grafting, by varying the initial ratio of rigid chains (λ). The results show that simultaneous grafting with a high fraction of rigid chains yields the highest grafting density, providing a pathway for optimizing the fabrication of high-density polymer brushes. In contrast, for the grafting-from strategy, with the rigidity range investigated in this study, increasing chain rigidity promotes more extended chain conformations, reduces the spatial shielding of surface initiation sites, and leads to polymer brushes with higher grafting density and lower dispersity. Overall, this study elucidates the mechanistic role of polymer chain rigidity in brush formation and provides theoretical guidance for the rational design and controlled fabrication of high-performance surface-modified materials through conformational regulation.

Keywords Grafting-from; Grafting-to; Chain rigidity; Polymer brushes; Coarse-grained molecular simulation

Citation: Zhang, Z. J.; Xu, W. S.; Ma, L. J.; Li, Y. X.; Guo, Y. Q.; Zhang, G. J.; Zhang, Z. Y.; Wang, Y.; Liu, H. Chain rigidity as a key regulator on grafting density and dispersity of polymer brushes: insights from coarse-grained molecular dynamics simulations. *Chinese J. Polym. Sci.* **2026**, *44*, 2305–2321.

INTRODUCTION

Polymeric materials play a pivotal role in modern science and industry. As the performance demands increase, surface modification has become a key area of research in polymer science. By tailoring the surface properties through physical or chemical approaches, surface modification can significantly enhance key characteristics, such as hydrophilicity, hydrophobicity, wear resistance, and antibacterial activity,[1,2] thereby greatly expanding the application scope of polymeric materials. For instance, in medical devices, surface modification enables polymeric materials to simultaneously exhibit antibacterial properties and biocompatibility, thereby facilitating the development of advanced medical products.[3,4] Common surface modification

* Corresponding authors, E-mail: zhangzhongyan@szbl.ac.cn (Z.Y.Z.)
E-mail: wangyan.cn@m.scnu.edu.cn (Y.W.)
E-mail: hongliu@m.scnu.edu.cn (H.L.)
† These authors contributed equally to this work.
Received December 31, 2025; Accepted January 30, 2026; Published online May 15, 2026

strategies include physical adsorption, chemical grafting, plasma treatment, and photochemical modification.[1,5] These approaches allow the precise tuning of surface properties according to specific material characteristics and application requirements, playing an essential role in polymer surface functionalization and engineering.

Polymer brushes represent a typical and highly important outcome of surface-modification technology. They consist of polymer chains tethered to a substrate through either physical adsorption or covalent bonding, extending outward to form brush-like architectures.[6–8] Structural parameters, such as chain length, rigidity, grafting density, and charge characteristics, strongly influence the resulting morphology and functional performance, thereby determining the surface properties of the material. Despite their nanoscale thickness, surface-grafted polymer layers can effectively regulate hydrophilicity or hydrophobicity and consequently impact biocompatibility and chemical stability. Owing to their ability to precisely control surface properties, polymer brushes have been widely applied in biomedicine,[9] electronics,[10] and biosensing.[11] In recent years, their application scope has expanded to emerging areas such as bio-lubrication, antifouling and antibacterial coatings, drug delivery, and bio-detection. Successful applications depend on precise control of the chemical composition, structure, and properties of polymer brushes, making them essential for high-performance surface engineering.[12–15]

The fabrication of polymer brushes generally involves three key steps: surface functionalization, introduction of active sites, and grafting of the polymer chains. Surface functionalization imparts a suitable chemical reactivity to the substrate, enabling stable and controllable grafting. Subsequently, active sites bearing specific functional groups are introduced to serve either as anchoring points for polymer chains or as initiators for controlled/living polymerization processes such as radical polymerization or atom transfer radical polymerization. Because the density and spatial distribution of these active sites determine the structure and properties of the resulting polymer brushes, this step is considered the most critical step in polymer brush synthesis. Active sites are commonly introduced by chemical or physical immobilization.[16] Chemical immobilization involves covalent bonding of active molecules onto substrates, such as silane coupling reactions on hydroxylated metal or metal oxide surfaces or thiol-based self-assembled monolayers on noble metals such as gold.[17,18] This approach offers excellent stability and precise control over the grafting density but often requires complex procedures and stringent reaction conditions.[19] In contrast, physical adsorption relies on non-covalent interactions, such as van der Waals forces, hydrogen bonding, and π-π interactions, but suffers from limited stability and reduced control over the active site distribution.[5,16]

The final step in polymer brush fabrication is the grafting of polymer chains onto the substrate surface, which can be classified into three primary strategies: “grafting to, “grafting from, and “grafting-through”.[5,20] In the grafting-to approach, pre-synthesized and well-characterized polymer chains are attached to the surface *via* reactions between their end-functional groups and surface-bound reactive sites.[16] This strategy allows for the use of polymers with narrow molecular weight distributions and well-defined structures, enabling the construction of brushes with precise architectures. Moreover, it is relatively straightforward to implement because it does not require polymerization to occur directly on the substrate.[5] However, steric hindrance arising from grafted chains significantly limits the achievable grafting density, especially for long polymer chains, thereby restricting the maximum attainable brush thickness.[20] Nevertheless, the grafting-to strategy remains valuable in applications where precise pre-characterization of polymer chains is required, and continues to be widely employed in surface and interface engineering.[7]

In contrast, the grafting-from strategy involves immobilizing polymerization initiators on the substrate surface and initiating polymer chain growth directly from the surface. Because chain growth proceeds outward, steric hindrance is substantially reduced, typically resulting in significantly higher grafting densities.[7] In addition, polymerization parameters, such as reaction time and monomer concentration, can be precisely controlled to regulate the chain length and brush thickness. This strategy is compatible with various polymerization mechanisms, including free radical, anionic, and ring-opening polymerization,[21–23] making it a versatile and powerful approach for preparing dense and structurally well-defined polymer brushes on diverse substrates. In contrast, the grafting-through strategy relies on the polymerization of macromonomers bearing polymeric side chains to directly generate brush architectures.[24] Although this approach allows good control over grafting density and structural regularity, the large steric hindrance and low effective concentration of macromonomers often make it difficult to obtain high-molecular-weight polymer brushes.

From an application perspective, ideal polymer brushes should simultaneously exhibit high grafting densities and low dispersities, which has long been a central objective in this field.[25,26] Surface-initiated atom transfer radical polymerization (SI-ATRP) has therefore been widely employed as an efficient and robust controlled/living radical polymerization technique for fabricating well-defined polymer brushes *via* a grafting-from strategy.[27] Numerous experimental and theoretical studies have demonstrated that polymerization conditions, initiator density, and reaction kinetics strongly influence the grafting density, dispersity, and final brush structure. Tsujii *et al*. investigated the factors influencing polymer brush formation during the surface-initiated polymerization of methyl methacrylate using Cu(I)Cl/Cu(II)Cl_2 or Cu(I)Br/Cu(II)Br_2 as the catalytic system.[28,29] Their results demonstrated that increasing the proportion of the deactivator significantly enhanced the grafting density and reduced the dispersity of the resulting brushes. From a theoretical perspective, Liu *et al*. employed molecular dynamics simulations to study the effects of the initiator density and polymerization rate on surface-initiated polymerization.[30] Their work revealed that both initiator density and polymerization rate substantially influence the final brush structure, initiation efficiency, and grafting density. In particular, under conditions of high initiator density or high polymerization rate, the obtained brushes often exhibit relatively large dispersity. Regarding the "graft-

https://doi.org/10.1007/s10118-026-3605-x

ing-to" strategy, Oyerokun *et al*. found that the average grafting density of polymer brushes adsorbed onto nanoparticle surfaces increases with a higher nanoparticle surface curvature or greater polymer chain concentration in solution.[31] Furthermore, the Barner-Kowollik group demonstrated that the grafting density is closely related to the radius of gyration of the polymer chains, which is significantly modulated by the solvent properties.[32] These findings highlight the importance of considering the physicochemical properties of the polymer chains during brush design and preparation.

Despite extensive efforts devoted to understanding polymer brush formation, the role of the intrinsic polymer chain properties, particularly chain rigidity, remains insufficiently explored. Polymer chain rigidity fundamentally governs conformational behavior and thus directly affects the brush morphology and performance. Research indicates[33] that flexible polymer chains typically adopt random coil conformations in both melt and solution states. When the chain concentration exceeded a critical value, these coils overlapped and further developed into an entangled network. In contrast, rigid chains tend to assume extended, rod-like conformations, resist entanglement, and exhibit physical behaviors distinct from those of their flexible counterparts. Chain rigidity is predominantly governed by the chemical structure of the monomer. For instance, structural elements, such as aromatic rings or conjugated backbones, severely restrict free bond rotation, leading to the formation of semi-rigid or rigid chains.[34] Furthermore, intermolecular hydrogen bonding or strong polar group interactions between monomer units (*e.g*., in cellulose and polyisocyanates) can significantly increase the rotational energy barrier, further enhancing the chain rigidity.[35] Notably, many polymer chains employed in surface modification inherently possess semi-flexible or rigid characteristics. For example, in polyisocyanates, intramolecular hydrogen bonding induces a helical conformation, rendering it a typical rigid-chain system with excellent insulation,[36] making it suitable for high-performance surface modification.[35] However, in surface-initiated polymerization processes, the impact of rigid chains (such as polyisocyanates) on the final properties of polymer brushes is often overlooked, and the underlying mechanisms require further exploration through theoretical modeling. Early work by Fredrickson *et al*. demonstrated that, compared to traditional flexible polymer brushes, rigid brushes exhibit markedly different characteristics, such as pronounced orientational order, weaker interchain interactions, and enhanced interfacial tension.[37] Consequently, these novel brushes based on rigid chains show broad application potential in fields such as organic photovoltaics, organic light-emitting diodes, low-friction coatings, fuel cell membranes, and high-performance protective coatings, surpassing the scope of traditional flexible brushes.[38,39] In summary, introducing rigidity into polymer chains not only fundamentally alters the intrinsic properties of polymer brushes but also opens new frontiers for their application.

A clear and quantitative understanding of how chain rigidity regulates grafting density, dispersity, and underlying microscopic mechanisms during polymer brush synthesis is still lacking. This challenge largely arises from the difficulty of directly probing the dynamic evolution of relevant physical quantities in experiments. To address this issue, the present study employed coarse-grained molecular dynamics simulations to systematically investigate the influence of polymer chain rigidity on brush formation *via* both grafting-from and grafting-to strategies. By analyzing the grafting density, dispersity, and chain conformations, this study elucidates the distinct roles of chain rigidity in different grafting processes and proposes effective design strategies for achieving high-performance polymer brushes. The results provide valuable theoretical insights and practical guidelines for the rational design and controlled fabrication of advanced surface modification materials through the precise manipulation of the polymer chain conformation.

MODELS AND SIMULATION METHOD

In the coarse-grained molecular dynamics simulations conducted in this study, Brownian dynamics under a canonical ensemble were employed, and an implicit solvent model was used to describe the motion of the polymer chains. The non-bonded interactions between any two coarse-grained beads were described by the Weeks-Chandler-Andersen (WCA) potential,[40] which is a truncated repulsive form of the Lennard-Jones potential that effectively captures the excluded-volume interactions between beads. The cut-off radius for the WCA potential was set to $r_c = 2^{1/6}\sigma$, where σ is the unit length. With this choice, only repulsive interactions were retained. Accordingly, solvent effects were treated implicitly through effective interactions, and the solvent quality was not independently varied in the present study.

$$U(r) = U_{LJ}(r) - U_{LJ}(r_c) \tag{1}$$

$$U_{LJ}(r) = \begin{cases} 4\varepsilon\left[\left(\frac{\sigma}{r}\right)^{12} - \left(\frac{\sigma}{r}\right)^{6}\right], & r \le r_c \\ 0, & r > r_c \end{cases} \tag{2}$$

where U (U_{LJ}) presents the pair potentials of the simulated systems, ε denotes the depth of the Lennard-Jones potential well, which characterizes the strength of the attractive interaction between particles. A larger ε corresponds to stronger intermolecular attraction, while a smaller value indicates weaker interactions. And σ is the characteristic distance at which the interparticle potential is zero.

The interactions between the two bonded beads were described using a bead-spring model. In this work, the following pairs were treated: adjacent monomers within a polymer chain and the active chain ends with an active site on the substrate. These bonded interactions are described by a harmonic spring potential, expressed as:

$$U_{bond} = \frac{1}{2}K_r(r - r_0)^2 \tag{3}$$

where K_r is the bond force constant controlling the stiffness of the bond, r is the instantaneous bond length, and r_0 is the equilibrium bond length. The spring constant was set to $K_r = 30k_BT/\sigma^2$, ensuring moderate bond fluctuations around r_0. The widely used FENE potential[41] was not employed because the harmonic spring potential offers better tolerance to initial conformations, facilitates the generation of random initial states, and provides more stable handling of bond-length variations

during new bond formation in the grafting process. For the equilibrium processes examined in this study, this choice did not affect the reliability of the simulation results. Our group previously compared the simulation results obtained with these two potential functions and found that the differences were negligible.[42]

During the grafting process, the rigidity of the polymer chains was modulated by adding a bending potential among three consecutive beads.[43,44] The bending potential is given by

$$U_\theta = \frac{1}{2}K_\theta[\cos(\theta) - \cos(\theta_0)]^2 \quad (4)$$

where θ is the instantaneous bond angle formed by three consecutive beads, θ_0 is the equilibrium bond angle, and K_θ is the bending force constant that determines the stiffness of the angle potential. A larger K_θ penalizes deviations from θ_0, resulting in stiffer chain conformations.

By adjusting the value of K_θ, the fluctuation amplitude of the bond angle could be controlled, thereby regulating the chain rigidity in the simulations. Physically, K_θ determines the energetic penalty associated with deviations from the equilibrium bond angle, and a larger K_θ suppresses bond-angle fluctuations and leads to stiffer, more extended chain conformations, whereas a smaller K_θ allows greater angular flexibility and corresponds to more flexible chains. In this study, K_θ=0, 5, and 50 were selected to qualitatively represent flexible, semi-rigid, and rigid polymer chains, respectively. In the present simulations, the chain rigidity was regulated through the intramolecular bond angle K_θ within an implicit solvent framework.

In the coarse-grained molecular dynamics simulations, the simulation box dimensions were set to $49.20\sigma \times 56.81\sigma \times 102.00\sigma$, with periodic boundary conditions applied in the x and y directions. The dimensions along the x- and y-directions were determined by the hexagonal arrangement of the grafting sites on the substrate surface.[42] This arrangement ensures uniform spacing between neighboring sites and avoids the influence of heterogeneity on the distribution of grafting sites. The unequal values of the dimensions along the x and y directions arise from the geometric constraints of the hexagonal packing, while the dimension along z direction was set to provide sufficient space for the grafting process in both the "grafting-to" and "grafting-from" strategies. Because this study focuses on the grafting behavior of polymer chains on a planar substrate, virtual repulsive walls were placed at the upper and lower boundaries along the z-direction to prevent beads from crossing. This configuration ensures that grafting reactions occur only within a specific region of the simulation box. Virtual repulsive walls[45] were implemented by imposing a repulsive potential along the z-direction on all beads in the system at the upper and lower z-boundaries:

$$U_{LJW} = 4\varepsilon\left[\left(\frac{\sigma}{r}\right)^{12} - \left(\frac{\sigma}{r}\right)^{6}\right], \quad (r < r_c) \quad (5)$$

where r is the shortest distance between a bead and the wall, ε represents the interaction strength between the bead and the wall, and σ is the characteristic length scale corresponding to the effective bead diameter. The cutoff distance was set to $r_c=2^{1/6}\sigma$, so that the potential is truncated at its minimum and becomes purely repulsive, corresponding to the Weeks-Chandler-Andersen (WCA) form.

All coarse-grained molecular dynamics simulations were performed using the GALAMOST software package.[46] The chemical reactions between the polymer chains and planar surface were handled by the SKIP-GALAMOST module.[47] In the simulations, the energy unit ε, length unit σ, and mass m of the coarse-grained beads were set as 1.0. The integration time step was set to $dt = 0.005\sigma(m/\varepsilon)^{1/2}$ and the simulation temperature was fixed at $T^* = 1.0k_BT/\varepsilon$.

Prior to initiating the grafting reactions, the system underwent simulations for approximately 2×10^5 time steps to achieve a fully relaxed and homogeneous initial structure. Subsequently, the grafting processes on the planar surface (including both "grafting-to" and "grafting-from") were simulated for the corresponding time steps in the different systems. It should be noted that during grafting simulations, a transient non-uniform pressure distribution within the system may occur, which could influence the local grafting reaction rate. However, the diffusion behavior of the polymer chains played a dominant role throughout the grafting process. Given that the system components remained homogeneously distributed for most of the simulation time, the overall impact of the local pressure fluctuations on the grafting process was not significant.

The grafting reactions ("grafting-to" and "grafting-from") were described using an algorithm proposed in our previous work.[47] This reaction model incorporates the reaction probability P_r to handle the bond formation. Within each grafting reaction time interval ($N_{step}\times dt$), a reaction radius (set equal to the cutoff radius in the WCA potential) was defined around the active site involved in the reaction. When an active free monomer is located within this reaction radius, the following steps are executed: (1) the program randomly selects a free monomer within the reaction radius, (2) a random number is generated, and if it is less than the preset P_r value, a grafting reaction occurs between the active free monomer and the active site, forming a new bond. Based on our previous study,[42] P_r was set to 0.1 to describe both types of grafting reactions. For details on the reaction kinetics and the quantitative relationship between the reaction probability and reaction rate, please refer to our previously published work.[47]

The coarse-grained model used to describe the "grafting-from" process involves two bead types: A and C. Type A beads represent the initiation sites on the substrate surface, whereas type C beads represent the active free monomers in the system. Type C beads can form covalent bonds with type A beads *via* free-radical polymerization. The specific reaction scheme is as follows.

$$A^* + C \rightarrow A - C^* \quad (6)$$

$$A - C^* + nC \rightarrow A - C_{n+1}{}^* \quad (7)$$

The coarse-grained model for the "grafting-to" process involves three bead types: A, B, and C. Type A beads represent the initiation sites on the substrate surface; type C beads constitute the polymer chains to be grafted; and type B beads serve as the active end groups that can form covalent bonds with type A beads *via* a free-radical polymerization reaction. The specific reaction scheme is as follows.

$$\text{Substrate} - A^{*} + {}^{*}BC_x \rightarrow \text{Substrate} - A - B - C_x \quad (8)$$

In both models corresponding to the "grafting-from" and "grafting-to" strategies, respectively, the substrate is placed at the bottom of the simulation box (on the *x*-*y* plane). By adjusting the dimensions of the simulation box in the *z*-direction, the (free) monomer concentration in each system was maintained at approximately $0.35\sigma^{-3}$. Schematic illustrations of the coarse-grained models of the two grafting processes are shown in Fig. 1.

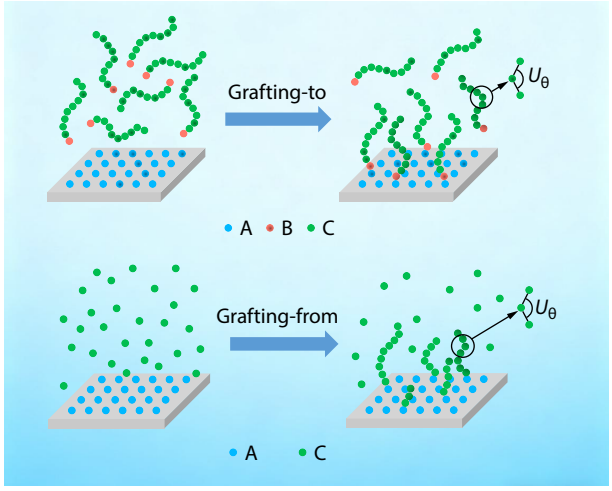

Fig. 1 Schematic illustration of the simulations for the "grafting-from" and "grafting-to" processes. In the "grafting-to" process, active sites on the substrate are also represented by blue beads, while polymer chains are composed of green and red beads, with the red beads denoting the active chain ends. In the "grafting-from" process, active sites on the substrate are represented by blue beads, and free monomers are represented by green beads. The chain rigid of the free polymer chains and growing polymer chains are controlled by U_θ.

RESULTS AND DISCUSSION

Fabrication of Rigid Polymer Brushes Using the Grafting-to Strategy

Polymer brush fabrication *via* the "grafting-to" strategy is intrinsically limited by steric hindrance arising from the polymer chains already grafted to the substrate surface. As grafted chains occupy an increasing surface area, they progressively hinder the access of free polymer chains to the available grafting sites, ultimately imposing an upper limit on the achievable grafting density. Because the extent of steric hindrance is closely related to the polymer chain conformation, chain rigidity is expected to play a critical role in regulating the grafting behavior. In this section, we therefore investigate how chain rigidity and other relevant parameters influence the grafting density of polymer brushes fabricated *via* the "grafting-to" strategy within this intrinsic limitation.

Herein, the maximum grafting density is defined as $\sigma_i = n_s/A$, where n_s is the number of grafting sites initially placed in the simulation system, and A is the area of the substrate. In the initial configuration, the number of free polymer chains in the system was set equal to the maximum grafting density. Our group's previous study[42] indicated that when σ_i>0.5, the grafting density of the resulting polymer brush no longer increased with further increases in the maximum grafting density. Therefore, in the subsequent investigation, the maximum grafting density was set to σ_i=1.14 sites/σ^2, a value significantly higher than that used in prior work. It should be noted that σ_i represents the maximum available grafting site density on the substrate in our model, serving as an upper bound for the reactive sites rather than the final grafting density. A relatively high σ_i was adopted to avoid an artificial site-limited regime and ensure that the grafting density was mainly governed by chain diffusion and grafting kinetics. Using a classic work,[48] we map 1σ=1.472 nm, σ_i=1.14 sites/σ^2 corresponds to 0.526 sites/nm^2. In practice, experimentally accessible surface reactive-site densities are typically on the order of 0.05–0.80 sites/nm^2.[49] Therefore, σ_i is used here as a sufficiently high upper bound to ensure that the final grafting densities are governed by steric and diffusion limitations intrinsic to the grafting process. The initial feeding concentration of the polymer beads is defined as $[M_{to}] = N_{bead}/V$, where N_{bead} is the total number of beads in the polymer chains initially placed in the system, and V is the volume of the simulation box. By controlling the number and chain length of the free polymer chains in the initial configurations of different systems, we constructed simulation systems with varying initial feeding concentrations of the polymer chains. We first investigated the variation in grafting density with simulation time in systems with different chain rigidities, as shown in Fig. 2. Fig. 2(a) displays the evolution of the grafting density (σ_g) during the grafting process for polymer chains with a molecular weight of N=20 and varying rigidities. In the initial stage of the reaction, owing to the absence of significant spatial crowding on the substrate surface, free polymer chains experience minimal steric hindrance and can readily approach and graft onto the surface, leading to a rapid increase in grafting density. As the reaction proceeds into the intermediate stage, the polymer chains grafted onto the surface impose considerable steric hindrance on the free chains in the system, making subsequent grafting more difficult. Thus, the rate of increase in grafting density slows noticeably. For the flexible grafted-chain system (K_θ=0), the grafting density remained relatively low within the same simulation timeframe (saturating around 0.24 chains/σ^2) and exhibited the smallest increase over time among all systems. Flexible chains possess high conformational freedom because of their ease of bending and rotation, tending to adopt conformations parallel to the substrate to reduce the free energy of the system. However, this conformation increases steric hindrance; flexible chains can cover unreacted initiation sites, thereby hindering further grafting of free chains. When the grafted chains exhibit a moderate degree of rigidity ($K_\theta \geq 5$), the grafting density is significantly higher than that of the flexible system. Notably, the system with K_θ=5 exhibits a unique behavior: its grafting density increases at a slower rate in the later stages of the simulation compared to other rigid systems, and its final grafting density is relatively lower. This may be attributed to the relatively low chain rigidity of this system, which causes it to partially resemble flexible chains in the later stages: the already-grafted chains, due to insufficient rigidity, cover adjacent ungrafted sites and inhibit subsequent grafting. Conse-

quently, the curve for the K_θ=5 system shows slowed growth in the later phase.

As seen in Fig. 2(a), at the simulation endpoint (8×10^7 time steps), the grafting densities of the rigid grafted-chain systems are 0.37, 0.38, 0.36, and 0.34 chains/σ^2, respectively, with room for further increase. Moderate chain rigidity facilitates the adoption of extended conformations perpendicular to the substrate, thereby reducing steric hindrance and allowing neighboring ungrafted sites to be utilized. Thus, systems with moderate chain rigidity demonstrated the potential for increased grafting density in the later simulation stages. This suggests that in the low-to-intermediate rigidity regime ($K_\theta \leq$ 50), steric shielding dominates the grafting behavior; more upright conformations reduce lateral site coverage and improve the accessibility of available grafting sites. In contrast, in the high-rigidity regime($K_\theta \geq 100$), the diffusion limitation becomes the controlling factor, as the mobility is strongly suppressed, leading to a reduced effective encounter rate between the free chains and the remaining grafting sites. The crossover between these two regimes accounts for the non-monotonic dependence of the grafting density on chain rigidity. However, when the grafted-chain rigidity is excessively high ($K_\theta \geq 100$), chain motion becomes restricted, slowing its diffusion toward ungrafted sites and resulting in a decrease in grafting density, a trend that becomes more pronounced with increasing rigidity. To further elucidate the influence of chain rigidity on grafting behavior, we selected two representative systems (K_θ=0 and K_θ=50) and visualized their grafting morphologies on a flat substrate using a reduced number of polymer chains for clarity. Fig. 2(b) shows the conformation of flexible polymer chains (K_θ=0) grafted onto the substrate surface, revealing collapsed chain conformations that exert a strong shielding effect on the surrounding grafting sites. Fig. 2(c) depicts the conformation of polymer chains with moderate rigidity (K_θ=50) after grafting, where the chains adopt a more extended configuration on the substrate and exhibit a weaker shielding effect on adjacent sites.

Previous studies have indicated that factors such as the initial feeding concentration of polymer chains, distribution of grafting sites, and molecular weight of the polymer chains all influence the grafting density of polymer brushes prepared *via* the "grafting-to" strategy.[42] To further elucidate the mechanisms of these factors, three representative grafted polymer chain systems with different rigidities were selected for in-depth investigation according to the definition introduced in the simulation model: K_θ=0 (flexible chain system), K_θ=5 (semi-rigid chain system), and K_θ=50 (rigid chain system). We monitored the final grafting density as a function of the initial polymer chain concentration in monodisperse systems with chain length N=20 for the same simulation time, and the results are shown in Fig. 3(a). At relatively low feeding concentrations ($[M_{to}] \leq 0.55\sigma^{-3}$), the grafting density of all the three systems increased with increasing concentration. However, as the feeding concentration continued to increase, the grafting density of the rigid chain system began to decrease and eventually fell below that of the semi-rigid system, although it remained higher than that of the flexible system. This trend indicates a non-monotonic dependence of

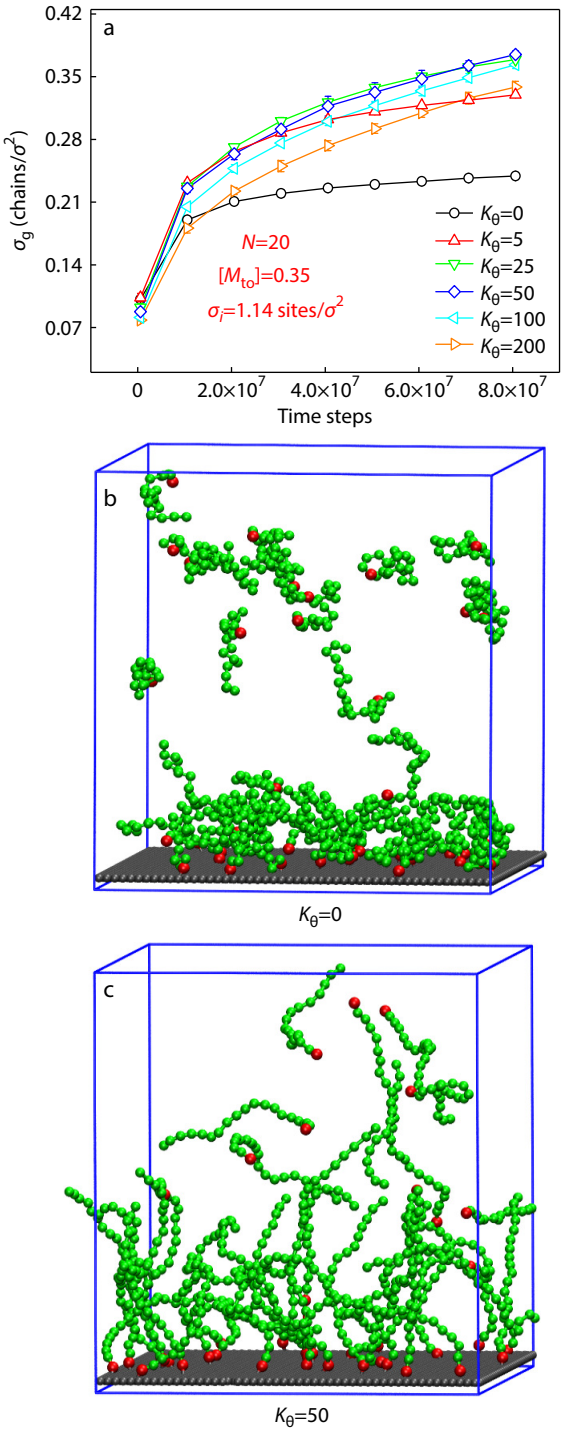

Fig. 2 (a) Grafting density as a function of time for polymer chains with different rigidities characterized by the bond-angle potential constant K_θ; (b) Snapshot of the grafting conformation for a flexible polymer chain (K_θ = 0); (c) Snapshot of the grafting conformation for a rigid polymer chain (K_θ = 50).

the grafting density on the initial feed concentration, particularly for systems with higher chain rigidity. This behavior can be primarily attributed to the lower diffusion rate of the free rigid chains, which reduces the probability of grafting to the substrate surface. When the feeding concentration was fur-

https://doi.org/10.1007/s10118-026-3605-x

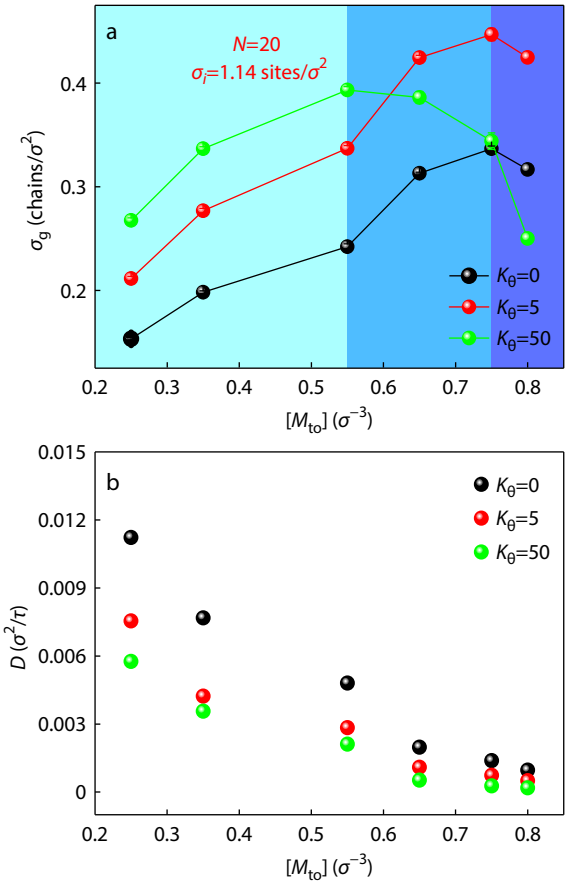

Fig. 3 Dependence of grafting density and polymer chain self-diffusion coefficient on initial feeding concentration [M_{to}], where [M_{to}] denotes the initial concentration of polymer beads in the simulation box. (a) Grafting density as a function of the initial feeding concentration [M_{to}]; (b) Self-diffusion coefficient D of polymer chains as a function of the initial feeding concentration [M_{to}], where D characterizes the mobility of polymer chains.

ther increased ([M_{to}]>0.75σ^{-3}), the grafting density of all three systems exhibited an inflection point, indicating that the grafting density passed through a maximum and then decreased with further increase in concentration. Notably, the rigid chain system showed a particularly pronounced decrease, with its grafting density even dropping below that of the flexible system under certain concentration conditions. This phenomenon can be explained by the free chain diffusion behavior: rigid chains possess lower mobility than flexible chains, effectively increasing the viscosity of the system. As the feeding concentration increased, this effect was amplified, significantly hindering the diffusion of free rigid chains within the system. Consequently, the frequency of effective collisions between the free active chain ends and grafting sites on the substrate surface is markedly reduced, the grafting kinetics are slowed, and the probability of grafting reactions decreases. Therefore, while increasing the feed concentration initially enhances the grafting density by increasing the availability of free chains, excessively high concentrations ultimately suppress chain diffusion, leading to a reduction in the grafting density.

Through the analysis of the relationship between the feeding concentration of polymer chains and the final grafting density of polymer brushes, we found that the chain rigidity significantly influenced the grafting density. Specifically, for systems with higher chain rigidity, increasing the feed concentration markedly reduced the diffusion rate of the free polymer chains. To further clarify the correlation between the grafting density trend in Fig. 3(a) and the mobility of the free chains, we monitored the self-diffusion coefficient (D) of the free polymer chains[50] as a function of the feeding concentration. The results are shown in Fig. 3(b). The mean squared displacement (MSD) of the free polymer chains is calculated based on the time evolution of the chain center-of-mass positions and characterizes the average squared displacement of the chains over time. The MSD is defined as:

$$\mathrm{MSD}(t) = \frac{1}{N}\sum_{i=1}^{N} |\boldsymbol{r}_i(t) - \boldsymbol{r}_i(0)|^2 \tag{9}$$

where N is the number of free polymer chains, t is the simulation time, and $\boldsymbol{r}_i(t)$ denotes the center of mass of the i^{th} free polymer chain. In the long-time limit, where the center of mass MSD exhibits a linear dependence on time, the self-diffusion coefficient D is related to the MSD as follows:[51]

$$D = \frac{1}{6}\lim_{t\to\infty}\frac{\mathrm{d}}{\mathrm{d}t}(\mathrm{MSD}) \tag{10}$$

where MSD is the mean square displacement of the center of mass of the polymer chain, and d/dt denotes the time derivative.

As shown in Fig. 3(b), the diffusion coefficient D for the free polymer chains in all three systems with different chain rigidities gradually decreased with increasing feeding concentration [M_{to}], indicating that a higher feeding concentration suppressed chain diffusion. Among them, the rigid chain system (K_θ=50) shows the most pronounced reduction in diffusion D in the high-concentration regime, which directly correlates with the sharp decrease in grafting density observed for the same system in Fig. 3(a). This clear correspondence confirms that grafting progressively enters a diffusion-limited regime at a high feed concentration for rigid chains. Specifically, although the diffusion coefficient of the rigid chain is already lower than that of the semi-rigid and flexible systems at low feeding concentrations ([M_{to}] ≤ 0.55 σ^{-3}), the mobility of all three systems remains sufficient to allow free chains to reach the substrate surface and complete grafting. However, as the feeding concentration increases further, the system becomes progressively more crowded, and the translational motion of the rigid chains is increasingly constrained by steric hindrance and frequent intermolecular collisions. This results in a rapid loss of mobility and thus a reduced probability of effective encounters between the active chain ends and the available surface grafting sites. Based on these results, controlling the feeding concentration to approximately 0.7 σ^{-3} and employing semi-rigid chains can yield polymer brushes with a relatively high grafting density. Therefore, grafting kinetics are co-regulated by multiple factors, including chain rigidity and feed concentration.

The grafting density of the polymer brushes is closely related to the molecular weight of the grafted polymer chains. To investigate this relationship, we examined the effects of chain rigidity and chain length (N=20, 30, 40, 50, 60) on grafting density at a fixed feeding concentration (approximately

https://doi.org/10.1007/s10118-026-3605-x

$0.35\sigma^{-3}$). The results are shown in Fig. 4(a). As observed in Fig. 4(a), the grafting density of all three systems decreased with increasing polymer chain length. This may be attributed to two reasons: first, as the molecular weight increases, the diffusion rate of free polymer chains in solution slows down, reducing their probability of reaching the substrate surface and undergoing grafting; second, after some polymer chains are grafted on the substrate surface, the steric hindrance generates shields surrounding grafting sites, inevitably affecting subsequent grafting. When the molecular weight of the polymer chain was relatively small (N<40), the grafting density gradually increased with the chain rigidity. This is because moderate chain rigidity can reduce the shielding effect of the already grafted chains on neighboring sites, thereby facilitating further grafting. However, as the molecular weight increased further (N>40), increasing the chain rigidity led to a decline in the grafting density. Under these conditions, the grafting density of the rigid system was lower than that of the semirigid system. This is because at higher molecular weights, increased chain rigidity significantly slows chain diffusion. Although rigid chains can mitigate the shielding effect, their negative impact on the diffusion rate dominates, resulting in an overall decrease in the grafting efficiency. In a simulation study of polymer chains grafted onto spherical nanoparticle surfaces, Liu *et al.*[42] indicated a linear scaling relationship between the grafting density and molecular weight, which can be estimated by linear fitting between $\ln(\sigma_g)$ and $\ln(N)$. To further quantitatively understand the relationship between the molecular weight and grafting density, we performed a double-logarithmic transformation of the data in Fig. 4(a), as shown in Fig. 4(b). Linear fitting of the data for systems with different chain rigidities yields the scaling relationship:

$$\sigma_g \sim < N >^{\gamma} \tag{11}$$

where γ is the scaling exponent. The γ values for the three systems are −0.62, −0.70, and −0.97, respectively. Fig. 4(b) shows a linear relationship between $\ln(\sigma_g)$ and $\ln(N)$. As the chain rigidity increased, the slope of the fitted line (*i.e.*, the γ value) decreased significantly (became more negative). The sign of γ reflects the positive or negative correlation between grafting density and molecular weight, while its absolute value indicates the sensitivity of grafting density to changes in molecular weight; a larger absolute value corresponds to higher sensitivity. The results in Fig. 4(b) show that the grafting density is negatively correlated with the chain length in all the systems, and the degree of this negative correlation strengthens with increasing chain rigidity. Combined with previous simulation results, it is evident that chain rigidity affects γ through multiple factors, including chain conformation and diffusion behavior. A well-defined scaling relationship exists between the grafting density and molecular weight in systems with different rigidities, and the scaling exponent γ is closely related to chain rigidity. Utilizing this scaling relationship allows for the effective prediction of the grafting density for systems with different molecular weights once the chain rigidity is known.

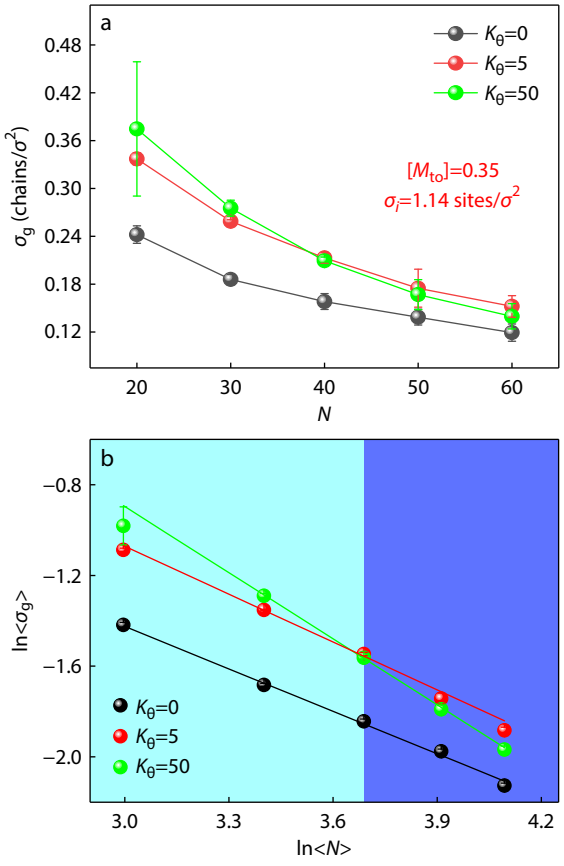

Fig. 4 Dependence of grafting density on the chain length N of the initially added polymer chains. (a) Grafting density as a function of chain length N; (b) Double-logarithmic plot of grafting density versus the chain length N of the initially added polymer chains. Solid circles represent simulation results, and the straight line represents a linear fit.

Increasing the density of grafting sites on the substrate surface is a common experimental strategy.[52] Accordingly, this study further investigated the relationship between the grafting density (σ_g) of polymer brushes and the grafting site density (σ_i) on the substrate surface. The results are shown in Fig. 5(a). As shown, the grafting density of the flexible polymer chain system (K_θ=0) remained relatively low, stabilizing at approximately 0.24 chains/σ^2 (black curve in Fig. 5a), and showed almost no variation with changes in σ_i. This is because the flexible chains generate strong steric hindrance, significantly shielding the surrounding grafting sites. Even when σ_i was increased, these sites remained covered by the already-grafted flexible chains, preventing an increase in the number of effective grafting sites. For systems with a certain degree of chain rigidity (red and green curves in Fig. 5a), the dependence of σ_g on σ_i can be divided into two regimes: in the low σ_i regime ($\sigma_i \leq 0.35$), σ_g increases significantly with σ_i, whereas in the high σ_i regime (σ_i>0.4), the increase in σ_g with σ_i slows considerably and gradually plateaus. At a low σ_i, the steric hindrance from the chains was not pronounced, and the grafting sites experienced minimal shielding, leading to a grafting efficiency close to 100%. However, once σ_i exceeds a certain threshold, steric hindrance from the grafted chains intensifies. Increasing σ_i effectively reduces the inter-site distance, making the shielding effect prominent, thereby suppressing subsequent grafting. Furthermore, Fig. 5(a) shows that the plateau value of σ_g increases with chain rigidity within the range studied, indicating that chain rigidity helps miti-

https://doi.org/10.1007/s10118-026-3605-x

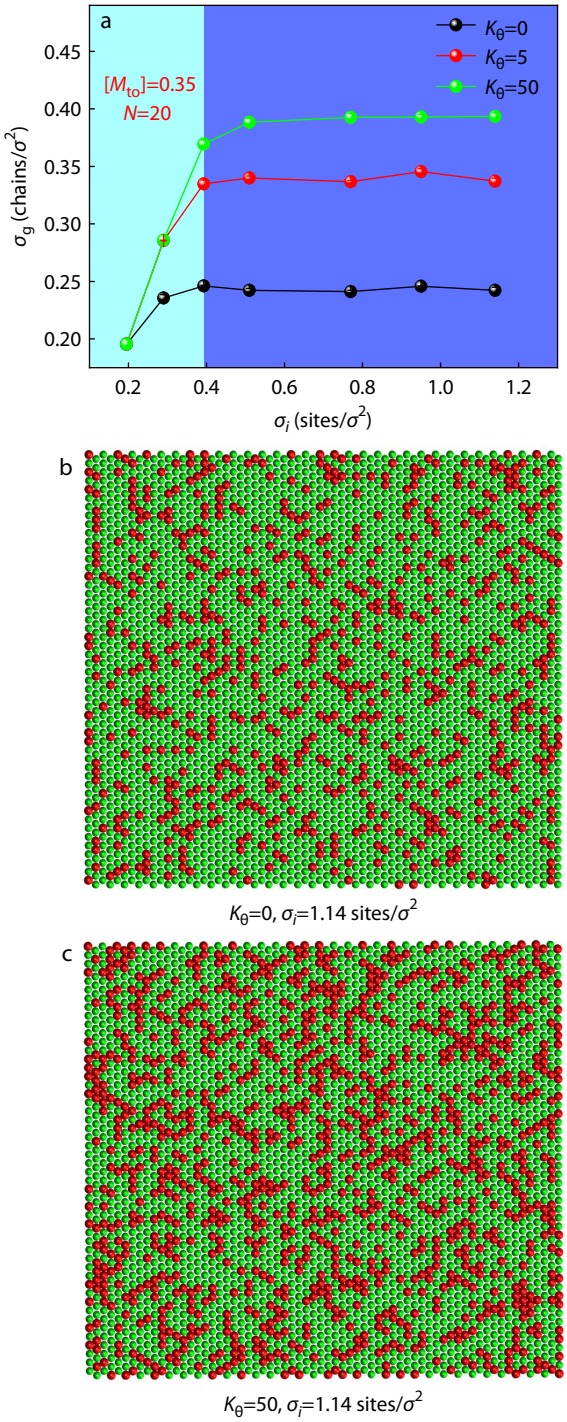

Fig. 5 (a) Grafting density σ_g as a function of grafting site density σ_i, where σ_g denotes the density of polymer chains grafted onto the substrate surface and σ_i represents the maximum grafting density determined by the initial density of grafting sites on the substrate; (b) Distribution of grafting sites on the substrate surface grafted with flexible polymer chains; (c) Distribution of grafting sites on the substrate surface grafted with rigid polymer chains. Green and red color represent ungrafted and grafted sites, respectively.

gate the shielding effect of chains on neighboring sites. To visualize the grafting status in systems with different chain rigidities, schematic diagrams are provided in Figs. 5(b) and 5(c), where the green and red dots represent ungrafted and grafted sites, respectively. It is clearly observed that the number of grafted sites (red) in the rigid chain system is substantially greater than that in the fully flexible system. Overall, these results demonstrate that introducing an appropriate degree of chain rigidity can effectively alleviate steric shielding effects and thereby facilitate higher grafting densities during the grafting-to process, particularly at high grafting site densities.

The design and fabrication of polymer brushes with high grafting densities remains a persistent objective in the grafting-to strategy. In the preceding sections, we systematically examined how chain rigidity influences the grafting density during the grafting-to process and investigated the effect of key physical factors on the grafting-to process.

Building on these insights, we now extend our investigation to a more complex and practically relevant scenario: binary polymer brushes composed of flexible and rigid chains grafted *via* the "grafting-to" strategy. In such systems, an additional question naturally arises: Given the distinct conformational and steric characteristics of flexible and rigid chains, how should the grafting process be organized to maximize the grafting density.

To address this question, we designed and compared three representative grafting strategies involving flexible chains (K_θ=0, denoted as F) and rigid chains (K_θ=50, denoted as R): (1) F/R strategy: flexible chains grafted onto the substrate prior to rigid chains; (2) R/F strategy: rigid chains grafted prior to flexible chains; and (3) both strategies: flexible and rigid chains graft simultaneously. The detailed simulation parameters for the three-strategy systems are listed in Table 1. Here, we define the initial rigid chain ratio as $\lambda = n_k/n_0$, where n_k is the number of rigid grafted polymer chains initially placed in the system and n_0 is the total number of grafted polymer chains initially placed. We monitored the variation in the grafting density with the parameter λ, and the results are presented in Fig. 6.

As shown in Fig. 6, the F/R strategy yielded the lowest grafting density. In this system, flexible chains were first grafted onto the substrate. Owing to their highly collapsible conformation, they generate significant steric hindrance and a shielding effect, covering a considerable number of unreacted grafting sites, thereby severely suppressing the subsequent grafting of rigid chains. The grafting density of the F/R system increases only slowly with λ, becoming comparable to the other two systems only when λ reaches its maximum. For both R/F and both systems, the grafting densities increase with λ at a rate significantly faster than that of the F/R system. When $\lambda \leq 0.5$, the grafting density of the R/F system increased slightly faster than those of both systems. However, when $\lambda > 0.5$, the growth rate of the grafting density for both systems surpassed that of the R/F system, exhibiting a stronger upward trend. This crossover behavior indicates that the higher grafting density of both systems at large λ arises from the combined effects of reduced site shielding by rigid chains and an increased effective density of the active chain ends. The dominant contribution comes from the simultaneous activation of both components, which allows more chains to graft during the initial stage when the grafting sites are still

https://doi.org/10.1007/s10118-026-3605-x

Table 1 Parameter settings for the preparation of binary polymer brushes under different grafting strategies.

Grafting strategy	Stage 1		Stage 2	
	Time (τ)	P_r (R) /P_r (F)	Time (τ)	P_r (R)/P_r (K)
F/R	4.0×10^7	P_r (R) = 0 P_r (F) = 0.1	4.0×10^7	P_r (R) = 0.1 P_r (F) = 0
R/F	4.0×10^7	P_r (R) = 0.1 P_r (F) = 0	4.0×10^7	P_r (R) = 0 P_r (F) = 0.1
Both	4.0×10^7	P_r (R) = 0.1 P_r (F) = 0.1	0	

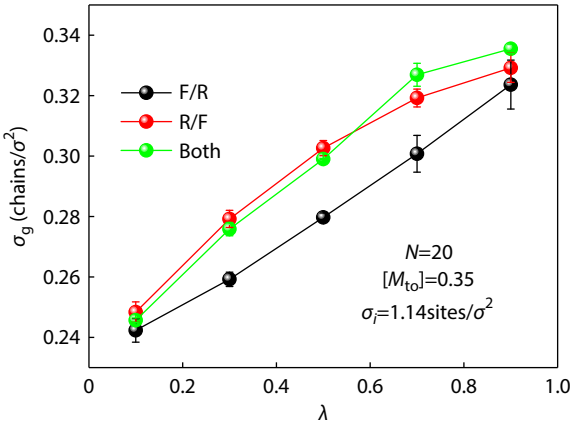

Fig. 6 Overall grafting density as a function of initial rigid chain ratio λ for the three systems, where λ represents the fraction of rigid polymer chains among the initially introduced grafted chains.

accessible, whereas in the R/F case, the later-activated chains experience stronger steric hindrance from the already formed brush layer. Overall, the grafting density values of the three systems were relatively similar when λ was at its minimum or maximum. However, their evolutionary paths diverged during the λ. At low λ values, the number of rigid chains in the system is small, and the grafting process is dominated by flexible chains. Owing to the strong spatial shielding effect exerted by the grafted flexible chains on neighboring sites, all three systems exhibited relatively low grafting densities at this stage. When λ was very high, the number of flexible chains in the system was minimal, and the grafting process was primarily driven by rigid chains, resulting in a high grafting density across all three systems. Theoretically, both systems, where rigid and flexible chains graft simultaneously, should possess a higher grafting density because of the higher density of the active chain ends. However, Fig. 6 shows that at low λ values, the grafting density of the R/F system is comparable to or even slightly higher than those of both systems. This can also be attributed to the site-shielding effect caused by flexible chains: in the both system, the flexible chains present initially still impose some shielding on the sites. At a low rigid-chain fraction (λ), although both strategies involve a higher instantaneous density of active chain ends, the presence of flexible chains during the early grafting stage leads to partial shielding of the neighboring surface sites because of their collapsed conformations. This spatial shielding reduces the effective accessibility of the grafting sites and limits the grafting efficiency in both systems. In contrast, in the R/F strategy, rigid chains graft first and adopt more extended conformations, which weakly shield the surrounding sites and preserve surface accessibility at early times. Consequently, the R/F system can achieve a comparable or even slightly higher grafted fraction than both systems at low λ, as quantitatively demonstrated in Fig. S2 (in electronic supplementary information, ESI). With increasing λ, the contribution of the rigid chains becomes dominant, and the higher density of simultaneously active chain ends in both strategies ultimately leads to a higher grafting density. As the proportion of rigid chains (λ) increased in both systems, the overall grafting density eventually exceeded that of the R/F system. Based on the above analysis, it can be inferred that in practical applications, by adjusting the ratio of rigid to flexible chains and adopting a co-grafting strategy, the site-shielding effect can be mitigated while improving the grafting efficiency, thereby effectively enhancing the final grafting density of the polymer brushes.

Fabrication of Rigid Polymer Brushes Using the Grafting-from Strategy

In the "grafting-from" strategy, the chain rigidity arises dynamically as the polymer chains grow from the substrate surface. The initial rigidity of the chains was determined by the intrinsic structures of the monomers. However, this rigidity is not fixed and can be modulated by environmental factors such as solvent quality and salt concentration. These factors influence the rigidity of the growing chains, which in turn affects the grafting process and final polymer brush density. Therefore, understanding the effect of chain rigidity on the grafting process is crucial for tailoring the properties of the resulting polymer brushes. Polymer brush fabrication *via* the "grafting-from" strategy is intrinsically prone to non-uniform chain growth owing to kinetic heterogeneity. This nonuniformity is intricately linked to both the rigidity of the growing chains and the dynamics of the polymerization process. Multiple factors can lead to the non-uniform growth of polymer brushes synthesized *via* the "grafting-from" strategy. First, after some grafted chains initiate and grow on the surface, they occupy adjacent regions and gradually form a thin-film-like structure. This film layer hindered the diffusion of free monomers from the solution to the surface-active sites for the reaction, thereby suppressing further chain propagation. Consequently, in the early stages of the grafting process, both unreacted active sites and short, "inactive" polymer chains can be observed on the surface. Second, within the initially formed polymer film, a small number of polymer chains with active ends continued to grow, achieving lengths significantly exceeding the average thickness of the film layer. Because of the relatively high concentration of free monomers above the film layer, these long chains continued to grow, eventually forming polymer chains with higher molecular weights. Different chain

https://doi.org/10.1007/s10118-026-3605-x

rigidities can lead to distinct chain conformations, which in turn affect the overall "grafting-from" process. Under the combined effects of these two mechanisms, polymer brushes prepared by surface-initiated polymerization inevitably exhibit a high dispersity. From an experimental characterization perspective, both the dispersity and grafting density of polymer brushes are key parameters for evaluating their performance.[53] The dispersity is typically defined as the ratio of the weight-average molecular weight (M_w) to the number-average molecular weight (M_n):

$$Đ = \frac{M_w}{M_n} = \frac{\sum_i N_i M_i^2 / \sum_i N_i M_i}{\sum_i N_i M_i / \sum_i N_i} \quad (12)$$

where M_i is the molecular weight of polymer chains in the i^{th} size class, and N_i is the number of chains with molecular weight M_i. The quantities M_w and M_n are the weight-average and number-average molecular weights, respectively, calculated from the molecular weight distribution of the system. The dispersity $Đ$ characterizes the breadth of the molecular weight distribution. In this study, we constructed a series of simulation systems to investigate the process of preparing polymer brushes *via* the "grafting-from" strategy. The free monomer concentration in the model system was set to $0.35\sigma^{-3}$. We defined the maximum grafting density as $\sigma_i = n_i / A$, where n_i is the number of initiator sites initially placed in the simulation system and A is the area of the substrate. In this work, σ_i was set to 0.77 initiators/σ^2. To investigate the influence of chain rigidity on the properties of the resulting polymer brushes, we assigned different rigidity parameters to polymer chains grown on the substrate. Fig. 7(a) illustrates the variation in dispersity with monomer conversion during polymer brush growth under different chain rigidity models. Here, monomer conversion is defined as: $X_m = N_i \times P_r^* \times t$, where N_i is the number of initiated initiators, $P_r^* = P_r \times [M]$ (P_r is the polymerization rate, [M] is the concentration of free monomers within the reaction radius of the initiator, and t is the reaction time). As shown in Fig. 7(a), when the monomer conversion increased from 10% to 70%, the dispersity of all the systems showed an upward trend. For flexible polymer brushes (K_θ=0), the dispersity increased rapidly from 1.44 to 1.85, whereas for brushes with a certain rigidity (K_θ>0), the dispersity increased only gradually with a smaller magnitude. This is because high-molecular-weight flexible chains are prone to collapse, thereby shielding the active ends of the surrounding shorter chains and temporarily deactivating them, leading to an increase in overall dispersity. In contrast, rigid chains tend to maintain an extended conformation perpendicular to the substrate during growth, which reduces the probability of their active ends being shielded by neighboring chains, resulting in more uniform growth

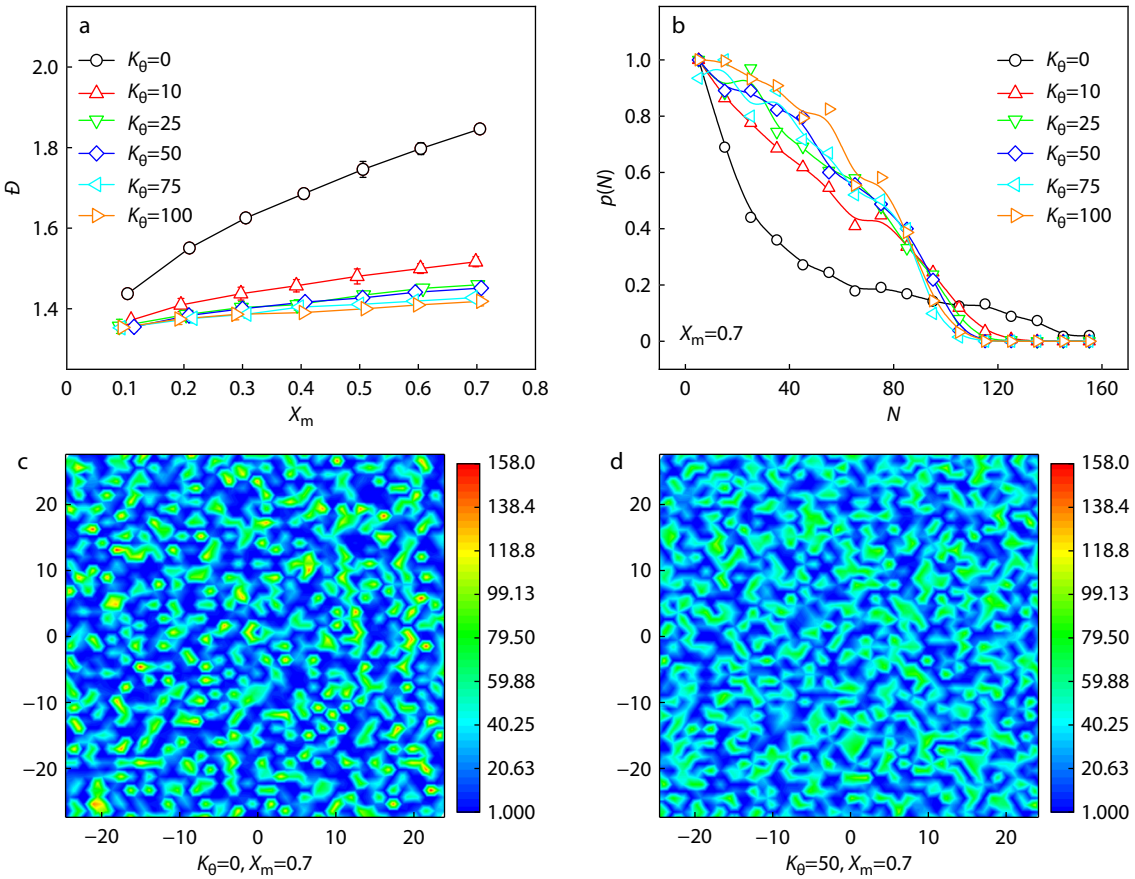

Fig. 7 During the grafting-from process at the maximum grafting density (σ_i=0.77): (a) Dispersity of polymer chains with different rigidities as a function of monomer conversion X_m, which represents the extent of monomer consumption during polymerization; (b) Probability distribution $p(N)$ of polymer chain lengths N with varying rigidities characterized by the bending constant K_θ. Each distribution is normalized by the maximum value of the chain length distribution for each rigidity; (c) Top view of local polymer length for a flexible polymer brush (growing flexible chains); (d) Top view of local polymer length for a rigid polymer brush (growing rigid chains).

https://doi.org/10.1007/s10118-026-3605-x

and a weaker tendency for an increase in dispersity. Furthermore, Fig. 7(a) indicates that as the polymer chain rigidity increased (with higher K_θ), the dispersity of the polymer brush slightly decreased. However, when the chain rigidity was further enhanced, no further significant reduction in dispersity was observed. This is because increasing the chain rigidity can only promote vertical chain growth to a limited extent; therefore, even with further increase in rigidity, the dispersity of the polymer brush cannot be effectively reduced further, as demonstrated in Fig. 7(a).

Subsequently, we analyzed the molecular weight distribution (MWD) of the growing polymer chains in systems with different chain rigidities at a free monomer conversion of X_m=70% (corresponding to the later stage of the simulation), which is labelled as the relationship of $p(N)$-N with $p(N)$ denoting the normalized ratio of grown polymers with a length of N. The results are shown in Fig. 7(b). As shown in Fig. 7(b), $p(N)$ underwent significant changes with increasing chain rigidity. Systems possessing a certain degree of rigidity (K_θ>0) exhibited a notably narrower $p(N)$ than a fully flexible system (K_θ=0). As the chain rigidity increased further, $p(N)$ continued to remain narrow, albeit with a diminishing rate of change. To more intuitively observe the growth morphology of the polymer brushes on the substrate surface in systems with different chain rigidities, we monitored the molecular weight of the polymer chains grafted at each initiator site. The results are presented in Figs. 7(c) and 7(d). In these figures, the x and y coordinates represent the spatial positions of the initiator sites on the grafting substrate, and the color scale indicates the molecular weight of the polymer chain at the corresponding site. Specifically, Fig. 7(c) corresponds to the case with flexible growing chains (K_θ=0), whereas Fig. 7(d) corresponds to the case with semi-rigid growing chains (K_θ=50). Fig. 7(c) reveals that in the flexible system, a considerable number of high molecular weight chains (red and yellow regions) were present, and their spatial distribution on the substrate was markedly heterogeneous. This is because the growing flexible chains shield the active ends of the neighboring shorter chains, allowing some initiated chains to grow continuously to a larger molecular weight, which is consistent with the high dispersity indicated by the black curve in Fig. 7(a). In contrast, Fig. 7(d) shows that in the system with rigid growing chains (K_θ=50), no exceptionally high-molecular-weight chains were observed (absence of red and yellow regions), and the polymer brushes exhibited a uniform distribution across the substrate surface. This is attributed to the weaker mutual shielding effect between the rigid chains, which allows the growth of individual chains to proceed relatively independently without significant interference. The results presented in Fig. 7 demonstrate that appropriately increasing the rigidity of the growing polymer chains helps reduce the dispersity of the polymer brushes, thereby improving their overall performance to a certain extent.

To further investigate the influence of chain rigidity on the structure of the growing polymer chains, we employed the radius of gyration (R_g) as a key physical parameter for the analysis.[54] The radius of gyration is given by the square root of the mean square radius of gyration, where the mean square value R_g^2 is expressed as

$$R_g^2 = \frac{1}{N}\sum_{i=1}^{N}(\boldsymbol{r}_i - \boldsymbol{r}_{cm})^2 \tag{13}$$

Here, N represents the number of monomers in the polymer chain, $\boldsymbol{r}_i$ is the position vector of the i^{th} monomer, and $\boldsymbol{r}_{cm}$ is the position vector of the center of mass of the chain. The mean square radius of gyration was obtained by calculating the squared distance between each monomer and the center of mass and averaging them. Furthermore, the degree of extension of the polymer chain is characterized by the chain stretch parameter Φ_s:[30]

$$\Phi_s = \frac{R_g^z}{\left[\frac{1}{2}\left(R_g^x + R_g^y\right)\right]} \tag{14}$$

In this expression, $R_g{}^x$, $R_g{}^y$, and $R_g{}^z$ are the components of the gyration radius along the x, y, and z directions, respectively. When Φ_s=1, the chain conformation is spherically symmetric; when Φ_s>1, the chain tends to grow preferentially in the direction perpendicular to the substrate. Thus, Φ_s serves as a valid metric for describing the extension behavior of the polymer chains.

To investigate the conformational evolution of the polymer chains during surface-initiated polymerization, we monitored the change in the radius of gyration (R_g) of the growing chains with simulation time, as shown in Fig. 8(a). It can be observed that R_g generally increases over time, primarily due to the increase in the degree of polymerization. Notably, the increase in R_g for flexible growing chains (K_θ=0) was significantly smaller than that for systems with a certain rigidity (K_θ>0), and R_g gradually increased with increasing chain rigidity. However, when K_θ≥50, a further increase in the chain rigidity resulted in a plateau in the growth trend of R_g. This behavior originates from the inherent physical characteristics of polymer chains; at a given molecular weight, the conformational restriction of the chain increases with rigidity, but this effect saturates in the high-rigidity regime, leading to the stabilization of R_g. Furthermore, we monitored the variation in the chain stretch parameter Φ_s for growing chains with different rigidities over the simulation time, as shown in Fig. 8(b). In the early stages of the reaction, when grafting density is low, the Φ_s values for all systems are close to 1, indicating that the polymer chains generally adopt a near-spherical "mushroom" conformation. In contrast, systems with K_θ>0 exhibit Φ_s values substantially greater than 1, suggesting that the rigid chains preferentially grow in the direction perpendicular to the substrate. As the reaction proceeds, Φ_s continues to increase, reflecting the rising grafting density and resulting crowded local environment, where interchain repulsion drives the transition from coiled to extended conformations. Compared to flexible systems, rigid systems consistently show higher Φ_s values, which increase progressively with rigidity. In the middle to late stages of the simulation, the growth of Φ_s in all systems with K_θ>0 slows significantly. This indicates that chain extension does not increase indefinitely; once the chains have reached a certain degree of extension, further increasing the chain rigidity does not substantially enhance their extension along the vertical direction.

Grafting density (σ_g) is a key parameter that influences the properties of polymer brushes. We analyzed the grafting density of the systems with different chain rigidities, and the re-

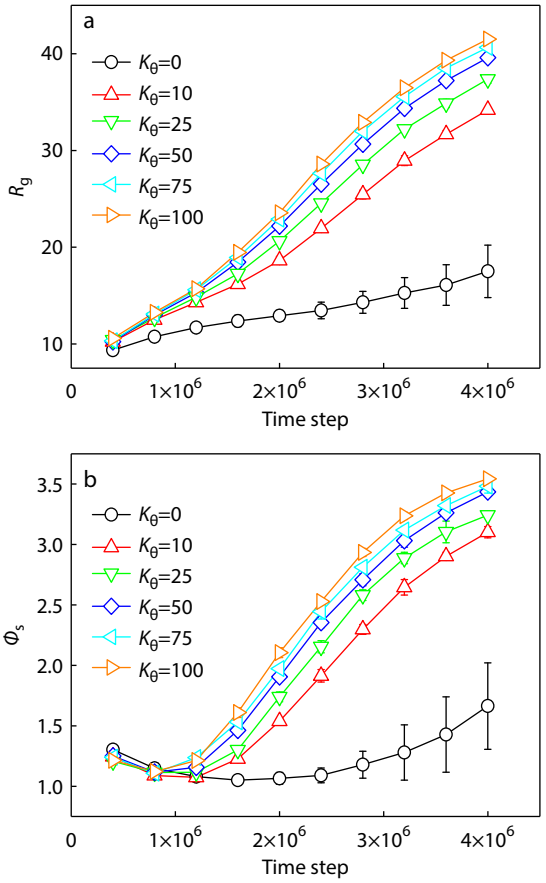

Fig. 8 Temporal evolution of the radius of gyration and the stretching coefficient for polymer chains with different rigidities at the maximum grafting density (σ_i=0.77). (a) The radius of gyration R_g as a function of time, where R_g characterizes the overall spatial extent of a polymer chain; (b) The chain stretch parameter Φ_s as a function of time, which quantifies the anisotropy of chain conformation by comparing chain extension normal to the substrate with that in the lateral directions.

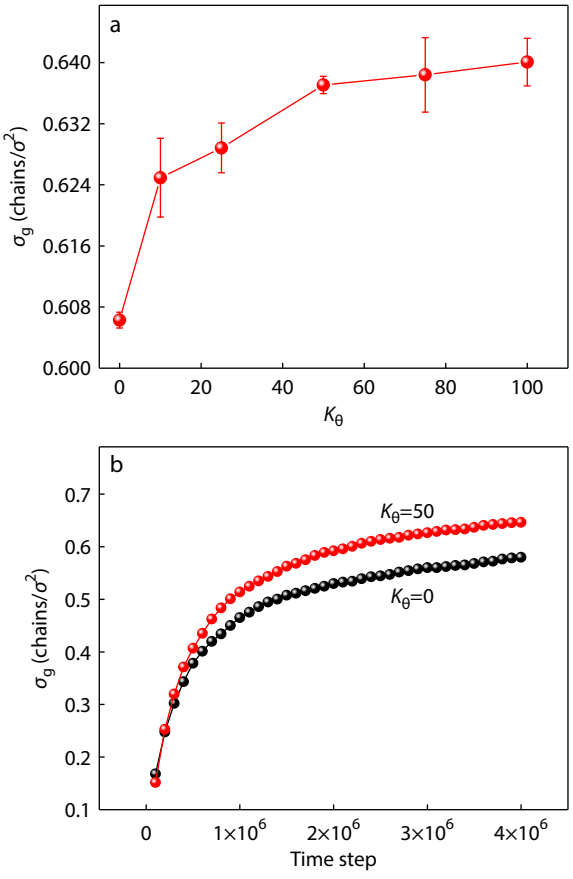

Fig. 9 Dependence of the grafting density of the polymer brush on chain rigidity and time at the maximum grafting density (σ_i=0.77). (a) Grafting density σ_g, defined as the surface number density of grafted polymer chains, as a function of the bond-angle potential constant K_θ, which characterizes chain rigidity; (b) Temporal evolution of the grafting density σ_g as a function of time for two representative rigidities, K_θ=0 (flexible chains) and K_θ=50 (rigid chains), during the grafting-from process.

sults are presented in Fig. 9. As shown in Fig. 9(a), the grafting density of the flexible polymer brush (K_θ=0) is approximately 0.60 chains/σ^2, while that of the rigid polymer brush (K_θ=50) is about 0.63 chains/σ^2. The grafting density increases with increasing chain rigidity, but the rate of increase gradually slows. When the chain rigidity exceeded a certain threshold ($K_\theta \geq 50$), the grafting density essentially stabilized, indicating that further increases in rigidity no longer significantly enhanced the utilization efficiency of the initiation sites. To further elucidate the mechanism by which the chain rigidity affects the grafting process, we selected two representative systems for comparative analysis: fully flexible chains (K_θ=0) and chains with moderate rigidity (K_θ=50). The evolution of the grafting density with the simulation time for these two systems is shown in Fig. 9(b). The results revealed that flexible and rigid growing chains exhibit different spatial screening effects on neighboring initiation sites during polymerization. In the early stages of the reaction, there was no significant difference in the grafting density between the two systems, as the initially formed polymer chains had low molecular weights and their screening effect was not yet pronounced. As the reaction proceeds and the molecular weight of the polymer chains increases, the chain segments in the flexible system are more prone to coiling and collapse, leading to strong spatial screening of adjacent initiation sites. This reduces the number of effectively available initiation sites, resulting in a noticeable decline in grafting density during the middle to late stages of the reaction.

The results in Fig. 9 indicate that the rigidity of the growing chains significantly affected the final grafting density of the polymer brushes. We previously defined free monomer conversion as $X_m = N_i \times P_r^* \times t$, where N_i is the number of initiated initiators, $P_r^* = P_r \times [M_{from}]$ (P_r is the polymerization rate, $[M_{from}]$ is the concentration of free monomers within the reaction radius of the initiated initiator, and t is the reaction time). In the current simulation system, the polymerization rate P_r is set as a constant; therefore, the monomer conversion can be simplified as $X_m = N_i \times [M_{from}] \times t$. Within a short simulation period, $N_i \times [M_{from}]$ can approximate the number of effective active chain ends in the system. To further investigate the mechanism by which chain rigidity influences the grafting density, we defined the effective active end ratio $\mu = (N_i \times$

$[M_{from}])/n_i$ (where n_i is the total number of initiators in the system). Analyzing the variation of μ with simulation time can more clearly reveal the accessibility of free monomers around the active chain ends. Fig. 10 shows the evolution of the monomer conversion (X_m) and effective active end ratio (μ) over the simulation time. Theoretically, given the same polymerization rate, the rigidity of the grafted chains should not affect free monomer conversion; thus, X_m should be essentially identical across different systems at any given time. As shown in Fig. 10(a), during the early stage of the reaction (0–5×10^5 time steps), the monomer conversion rates of the two systems indeed overlap closely, indicating that chain rigidity does not exert a significant influence on this phase. However, as the reaction proceeded, the gap in the conversion between the flexible and rigid chain systems widened gradually. Fig. 10(b) reveals that the effective active end ratio μ of the flexible chain system remained consistently lower than that of the rigid chain system throughout the polymerization process. This difference directly leads to a divergence in the conversion rate (Fig. 10a). The flexible chains generate

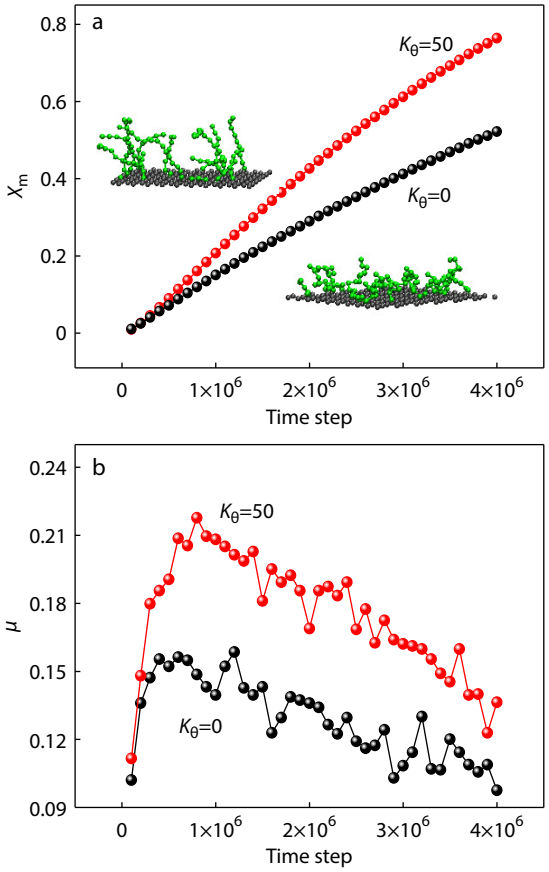

Fig. 10 Temporal evolution of free monomer conversion and the percentage of effective active chain ends for two representative chain rigidities, K_θ=0 (flexible chains) and K_θ=50 (rigid chains). (a) Free monomer conversion X_m, representing the fraction of free monomers consumed during grafting-from process, as a function of time; (b) Effective active end ratio μ as a function of time, where μ quantifies the fraction of initiators that are effectively active in chain growth by reflecting the accessibility of free monomers around active chain ends.

greater steric hindrance during growth, which reduces the proportion of effective active chain ends and consequently amplifies the heterogeneity in molecular weight among the chains. As shown in Fig. 7(a), the higher dispersity observed in the flexible chain system can also be attributed to steric hindrance effects reflected by the lower effective active end ratio. Furthermore, the μ values for both systems decreased over time, primarily because of the continuous consumption of free monomers.

Based on the above simulation results, it can be concluded that when employing the "grafting-from" strategy to synthesize polymer brushes, a certain degree of chain rigidity in the growing chains favors the maintenance of an extended conformation. This reduces the spatial shielding effect on the neighboring initiation sites, ultimately yielding polymer brushes with lower dispersity and higher grafting density. In practical applications, selecting appropriate monomers to modulate the rigidity of the growing chains is a viable strategy for the controlled synthesis of polymer brushes that simultaneously exhibit low dispersity and high grafting density.

A direct comparison between the grafting-to and grafting-from strategies reveals the fundamentally different roles of polymer chain rigidity. In the grafting-to process, polymer chains must diffuse from the solution to the surface and penetrate the grafted layer; thus, chain rigidity primarily affects grafting behavior through diffusion limitation and steric hindrance. Moderate rigidity can facilitate chain extension, whereas excessive rigidity restricts chain mobility and suppresses the grafting density. In contrast, the grafting-from strategy is dominated by the growth of surface-anchored chains rather than by chain transport. Here, chain rigidity mainly regulates grafting density and dispersity through growth heterogeneity and site shielding, as stiffer chains adopt more extended conformations that reduce the shielding of neighboring initiation sites. These differences highlight the fact that chain rigidity influences grafting outcomes *via* distinct physical mechanisms in the two strategies.

CONCLUSIONS

Polymer grafting is a pivotal strategy for surface functionalization, in which the grafting density of polymer brushes plays a decisive role in determining the surface modification performance. However, many key parameters governing the grafting process are difficult to quantify accurately experimentally. To address this challenge, this work systematically investigated polymer grafting-onto substrate surfaces *via* both the "grafting-from" and "grafting-to" strategies by combining coarse-grained molecular dynamics simulations with a stochastic reaction model. Particular emphasis was placed on elucidating the influence of the polymer chain rigidity on the grafting process. By analyzing key metrics, such as grafting density and product dispersity, this study provides mechanistic insights and practical guidelines for the experimental fabrication of high-performance polymer brushes.

In the case of the "grafting-to" strategy, the results indicate that, within an appropriate rigidity range, a moderate increase in chain rigidity is favorable for enhancing the grafting density. However, when the chain rigidity exceeds a critical threshold, the restricted chain mobility hinders adsorption

https://doi.org/10.1007/s10118-026-3605-x

and coupling to surface sites, leading to a reduction in the grafting density. In addition, the effects of initial polymer chain length, polymer concentration, and surface grafting site density were systematically examined. The grafting density decreased with increasing chain length, exhibited a non-monotonic dependence on the polymer concentration, and increased before reaching a plateau as the grafting site density increased. These findings highlight that the grafting process is governed by the coupled effects of multiple factors rather than by a single parameter. Furthermore, to enhance the grafting density of the binary polymer brushes using the "grafting-to" strategy, optimization was achieved by jointly tuning the chain rigidity and grafting sequence. Specifically, the flexible-first/rigid-second (F/R) strategy resulted in the lowest grafting density owing to pronounced shielding by the initially grafted flexible chains, whereas the rigid-first/flexible-second (R/F) strategy alleviated this limitation. The simultaneous grafting of rigid and flexible chains (both) further enhanced the grafting density, particularly at higher fractions of rigid chains.

For the "grafting-from" strategy, the simulations demonstrate that polymer chains with appropriate rigidity tend to adopt more extended conformations during growth, thereby effectively reducing the spatial shielding of surface initiation sites. Consequently, polymer brushes with lower dispersities and higher grafting densities can be achieved. By introducing the concept of effective active chain ends and analyzing their spatial distribution, we further revealed that increased chain rigidity promotes a more uniform and denser grafting process.

Overall, these results indicate that polymer chain rigidity should be tuned according to the specific grafting strategy employed. In the "grafting-to" approach, chain rigidity primarily influences grafting efficiency through its impact on chain diffusion and steric hindrance, such that excessive rigidity limits chain diffusion toward the substrate and suppresses grafting density. In contrast, in the "grafting-from" strategy, chain rigidity mainly governs the accessibility of free monomers to active chain ends and the extent of spatial shielding during chain growth, where an appropriate level of rigidity facilitates more extended conformations and sustains effective polymerization. This clear distinction highlights that chain rigidity does not play a universal role, but instead acts through different mechanisms in the grafting-to and grafting-from processes, providing important guidance for the rational selection of chain conformational properties in polymer brush design.

In summary, for practical applications that require polymer brushes with high grafting densities, it is advantageous to employ relatively low polymer concentrations and moderate surface grafting site densities. Moreover, under appropriate conditions, introducing suitable chain rigidity, such as through modulation of salt concentration or application of external fields, can further improve grafting efficiency. Increasing the proportion of rigid chains and adopting a simultaneous grafting approach are particularly effective for the preparation of binary polymer brushes using the "grafting-to" strategy. Overall, this work clarifies the critical role of polymer chain rigidity in brush synthesis and provides a theoretical foundation for the rational design and controlled fabrication of surface-modified materials through the deliberate regulation of chain conformational properties.

Conflict of Interests

The authors declare no interest conflict.

Electronic Supplementary Information

Electronic supplementary information (ESI) is available free of charge in the online version of this article at http://doi.org/10.1007/s10118-026-3605-x.

Data Availability Statement

The data that support the findings of this study are available from the corresponding author upon reasonable request. The author's contact information: hongliu@m.scnu.edu.cn.

ACKNOWLEDGMENTS

This work was financially supported by the National Natural Science Foundation of China (Nos. 22473046, 22273027, 22373024, 22503036, 22573021 and 22403059), and the Natural Science Foundation of Guangdong Province (No. 2025A1515010731). Hong Liu gratefully acknowledges support from the Alexander von Humboldt Foundation.

REFERENCES

1 Nemani, S. K.; Annavarapu, R. K.; Mohammadian, B.; Raiyan, A.; Heil, J.; Haque, M. A.; Abdelaal, A.; Sojoudi, H. Surface modification of polymers: methods and applications. *Adv. Mater. Interfaces* **2018**, *5*, 1801247.
2 Liu, T. L.; Kim, C. J. C. Turning a surface superrepellent even to completely wetting liquids. *Science* **2014**, *346*, 1096–1100.
3 Yoshida, S.; Hagiwara, K.; Hasebe, T.; Hotta, A. Surface modification of polymers by plasma treatments for the enhancement of biocompatibility and controlled drug release. *Surf. Coat. Technol.* **2013**, *233*, 99–107.
4 Goddard, J. M.; Hotchkiss, J. Polymer surface modification for the attachment of bioactive compounds. *Prog. Polym. Sci.* **2007**, *32*, 698–725.
5 Sun, W.; Liu, W.; Wu, Z.; Chen, H. Chemical surface modification of polymeric biomaterials for biomedical applications. *Macromol. Rapid Commun.* **2020**, *41*, 1900430.
6 Cosgrove, T.; Heath, T. G.; Ryan, K.; Crowley, T. L. Neutron scattering from adsorbed polymer layers. *Macromolecules* **1987**, *20*, 2879–2882.
7 Brittain, W. J.; Minko, S. A structural definition of polymer brushes. *J. Polym. Sci., Part A: Polym. Chem.* **2007**, *45*, 3505–3512.
8 Tirrell, M.; Patel, S.; Hadziioannou, G. Polymeric amphiphiles at solid-fluid interfaces: Forces between layers of adsorbed block copolymers. *Proc. Natl. Acad. Sci. U. S. A.* **1987**, *84*, 4725–4728.
9 Wu, B.; Feng, E.; Liao, Y.; Liu, H.; Tang, R.; Tan, Y. Brush-modified hydrogels: Preparations, properties, and applications. *Chem. Mater.* **2022**, *34*, 6210–6231.
10 Poisson, J.; Polgar, A. M.; Fromel, M.; Pester, C. W.; Hudson, Z. M. Preparation of patterned and multilayer thin films for organic electronics *via* oxygen-tolerant SI-PET-RAFT. *Angew. Chem. Int. Ed.* **2021**, *60*, 19988–19996.

Graphical Abstract

Chain Rigidity as a Key Regulator on Grafting Density and Dispersity of Polymer Brushes: Insights from Coarse-Grained Molecular Dynamics Simulations

Zheng-Jie Zhang, Wei-Shao Xu, Li-Jun Ma, Ying-Xiang Li, Yu-Qi Guo, Guo-Jie Zhang, Zhong-Yan Zhang, Yan Wang, and Hong Liu

South China Normal University; South China Normal University; Institute of Systems and Physical Biology, Shenzhen Bay Laboratory; Dongguan HEC Tech R&D Co., Ltd.; Guangzhou University; Lyuliang University

This study investigates how polymer chain rigidity affects grafting density. In "grafting-to," rigidity influences chain diffusion and grafting probability, while in "grafting-from," it controls active site accessibility.

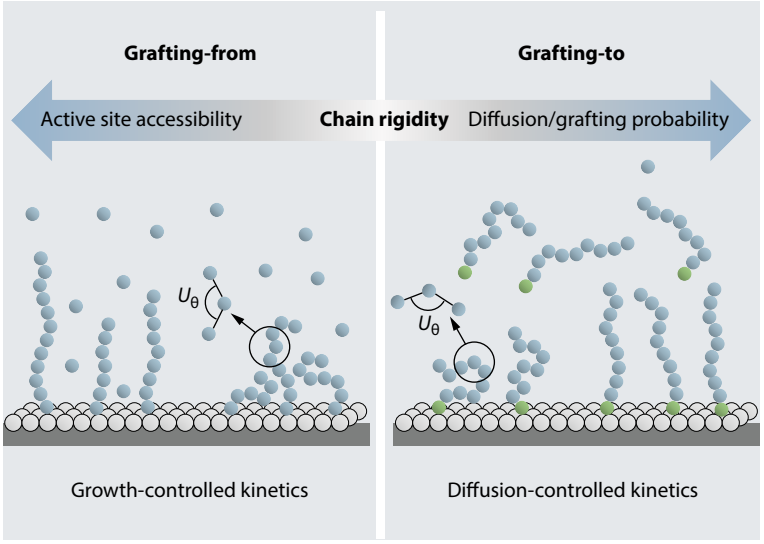

Chinese J. Polym. Sci. 2026, 44, 2305–2321 *https://doi.org/10.1007/s10118-026-3605-x*

11 Li, D.; Xu, L.; Wang, J.; Gautrot, J. E. Responsive polymer brush design and emerging applications for nanotheranostics. *Adv. Healthc. Mater.* **2021**, *10*, 2000953.
12 Inoue, Y.; Nakanishi, T.; Ishihara, K. Elastic repulsion from polymer brush layers exhibiting high protein repellency. *Langmuir* **2013**, *29*, 10752–10758.
13 Yoshikawa, C.; Sakakibara, K.; Nonsuwan, P.; Yamazaki, T.; Tsujii, Y. Nonbiofouling coatings using bottlebrushes with concentrated polymer brush architecture. *Biomacromolecules* **2021**, *22*, 2505–2514.
14 Li, T.-H.; Yadav, V.; Conrad, J. C.; Robertson, M. L. Effect of dispersity on the conformation of spherical polymer brushes. *ACS Macro Lett.* **2021**, *10*, 518–524.
15 Wang, C. G.; Chen, C.; Sakakibara, K.; Tsujii, Y.; Goto, A. Facile fabrication of concentrated polymer brushes with complex patterning by photocontrolled organocatalyzed living radical polymerization. *Angew. Chem. Int. Ed.* **2018**, *57*, 13504–13508.
16 Zdyrko, B.; Luzinov, I. Polymer brushes by the "grafting to" method. *Macromol. Rapid Commun.* **2011**, *32*, 859–869.
17 Julthongpiput, D.; Lin, Y. H.; Teng, J.; Zubarev, E. R.; Tsukruk, V. V. Y-shaped amphiphilic brushes with switchable micellar surface structures. *J. Am. Chem. Soc.* **2003**, *125*, 15912–15921.
18 LeMieux, M. C.; Julthongpiput, D.; Bergman, K. N.; Cuong, P. D.; Ahn, H.-S.; Lin, Y. H.; Tsukruk, V. V. Ultrathin binary grafted polymer layers with switchable morphology. *Langmuir* **2004**, *20*, 10046–10054.
19 Tobiesen, F. A.; Michielsen, S. Method for grafting poly(acrylic acid) onto nylon 6, 6 using amine end groups on nylon surface. *J. Polym. Sci., Part A: Polym. Chem.* **2002**, *40*, 719–728.
20 Henze, M.; Mädge, D.; Prucker, O.; Rühe, J. "Grafting through": mechanistic aspects of radical polymerization reactions with surface-attached monomers. *Macromolecules* **2014,** *47*, 2929–2937.
21 Wang, J.-S.; Matyjaszewski, K. Controlled/" living" radical polymerization. atom transfer radical polymerization in the presence of transition-metal complexes. *J. Am. Chem. Soc.* **1995**, *117*, 5614–5615.
22 Tsoukatos, T.; Pispas, S.; Hadjichristidis, N. Complex macromolecular architectures by combining TEMPO living free radical and anionic polymerization. *Macromolecules* **2000**, *33*, 9504–9511.
23 Sato, T.; Dunderdale, G. J.; Hozumi, A. Threshold of surface initiator concentration for polymer brush growth by surface-initiated atom transfer radical polymerization. *Langmuir* **2023**, *40*, 480–488.
24 Mohammadi Sejoubsari, R.; Martinez, A. P.; Kutes, Y.; Wang, Z.;

Dobrynin, A. V.; Adamson, D. H. "Grafting-through": growing polymer brushes by supplying monomers through the surface. *Macromolecules* **2016,** *49*, 2477–2483.
25 Liu, S.; Motta, A.; Mouat, A. R.; Delferro, M.; Marks, T. J. Very large cooperative effects in heterobimetallic titanium-chromium catalysts for ethylene polymerization/copolymerization. *J. Am. Chem. Soc.* **2014**, *136*, 10460–10469.
26 Pester, C. W.; Benetti, E. M. Modulation of polymer brush properties by tuning dispersity. *Adv. Mater. Interfaces* **2022**, *9*, 2201439.
27 Zhang, Z.; Li, H.; Guo, Y.; Xue, Y.-H.; Liu, H. Influence of activation/deactivation process on surface-initiated atom transfer radical polymerization: an in silico investigation. *Giant* **2025**, *21*, 100345.
28 Hsu, S.-Y.; Kayama, Y.; Ohno, K.; Sakakibara, K.; Fukuda, T.; Tsujii, Y. Controlled synthesis of concentrated polymer brushes with ultralarge thickness by surface-initiated atom transfer radical polymerization under high pressure. *Macromolecules* **2019**, *53*, 132–137.
29 Hsu, S.-Y.; Ohno, K.; Sakakibara, K.; Tsujii, Y. Convenient synthesis of very-thick concentrated polymer brushes by atom transfer radical polymerization in an ionic liquid. *Macromolecules* **2020**, *53*, 7936–7943.
30 Liu, H.; Li, M.; Lu, Z. Y.; Zhang, Z. G.; Sun, C. C. Influence of surface-initiated polymerization rate and initiator density on the properties of polymer brushes. *Macromolecules* **2009**, *42*, 2863–2872.
31 Oyerokun, F. T.; Vaia, R. A. Distribution in the grafting density of end-functionalized polymer chains adsorbed onto nanoparticle surfaces. *Macromolecules* **2012**, *45*, 7649–7659.
32 Michalek, L.; Barner, L.; Barner-Kowollik, C. Polymer on top: Current limits and future perspectives of quantitatively evaluating surface grafting. *Adv. Mater.* **2018**, *30*, 1706321.
33 Ballauff, M. Stiff-chain polymers—structure, phase behavior, and properties. *Angew. Chem. Int. Ed.* **1989**, *28*, 253–267.
34 Ronova, I.; Ponomarev, I. Design of monomeric units for rigid aromatic polymers. *Struct. Chem.* **2019**, *30*, 1611–1627.
35 Lim, E.; Tu, G.; Schwartz, E.; Cornelissen, J. J.; Rowan, A. E.; Nolte, R. J.; Huck, W. T. Synthesis and characterization of surface-initiated helical polyisocyanopeptide brushes. *Macromolecules* **2008**, *41*, 1945–1951.
36 Golling, F. E.; Pires, R.; Hecking, A.; Weikard, J.; Richter, F.; Danielmeier, K.; Dijkstra, D. Polyurethanes for coatings and adhesives–chemistry and applications. *Polym. Int.* **2019**, *68*, 848–855.
37 Morse, D. C.; Fredrickson, G. H. Semiflexible polymers near interfaces. *Phys. Rev. Lett.* **1994**, *73*, 3235.
38 Prehn Jr, F. C.; Boyes, S. G. Surface-initiated chain growth polyaramid brushes. *Macromolecules* **2015**, *48*, 4269–4280.
39 Okamoto, K.; Luscombe, C. K. Controlled polymerizations for the synthesis of semiconducting conjugated polymers. *Polym. Chem.* **2011**, *2*, 2424–2434.
40 Weeks, J. D.; Chandler, D.; Andersen, H. C. Role of repulsive forces in determining the equilibrium structure of simple liquids. *J. Chem. Phys.* **1971**, *54*, 5237–5247.
41 Kremer, K.; Grest, G. S. Dynamics of entangled linear polymer melts: A molecular-dynamics simulation. *J. Chem. Phys.* **1990**, *92*, 5057–5086.
42 Liang, C. X.; Lu, H.; Huang, B. Y.; Xing, J. Y.; Gu, F. L.; Liu, H. Physical insight for grafting polymer chains onto the substrate *via* computer simulations: kinetics and property. *Chinese J. Polym. Sci.* **2022**, *40*, 817–833.
43 Pei, H. W.; Liu, H.; Lu, Z. Y.; Zhu, Y. L. Tuning surface wettability by designing hairy structures. *Phys. Rev. E* **2015**, *91*, 020401.
44 Wang, Y.; Lu, H.; Jia, X.-M.; Shi, A.-C.; Zhou, J.; Zhang, G.; Liu, H. Entropy-induced localization and sliding dynamics of rings on polyrotaxane. *Macromolecules* **2024**, *57*, 1846–1858.
45 Magda, J.; Tirrell, M.; Davis, H. Molecular dynamics of narrow, liquid-filled pores. *J. Chem. Phys.* **1985**, *83*, 1888–1901.
46 Zhu, Y. L.; Liu, H.; Li, Z. W.; Qian, H. J.; Milano, G.; Lu, Z. Y. GALAMOST: GPU-accelerated large-scale molecular simulation toolkit. *J. Comput. Chem.* **2013**, *34*, 2197–2211.
47 Liu, H.; Zhu, Y. L.; Lu, Z. Y.; Müller-Plathe, F. A kinetic chain growth algorithm in coarse-grained simulations. *J. Comput. Chem.* **2016**, *37*, 2634–2646.
48 Buehler, M. J. Atomistic and continuum modeling of mechanical properties of collagen: elasticity, fracture, and self-assembly. *J. Mater. Res.* **2006**, *21*, 1947–1961.
49 Zoppe, J. O.; Ataman, N. C.; Mocny, P.; Wang, J.; Moraes, J.; Klok, H. A. Surface-initiated controlled radical polymerization: state-of-the-art, opportunities, and challenges in surface and interface engineering with polymer brushes. *Chem. Rev.* **2017**, *117*, 1105–1318.
50 Waseda, Y. The structure of non-crystalline materials. *Liquids and Amorphous Solids* **1980**.
51 Nagai, T.; Tsurumaki, S.; Urano, R.; Fujimoto, K.; Shinoda, W.; Okazaki, S. Position-dependent diffusion constant of molecules in heterogeneous systems as evaluated by the local mean squared displacement. *J. Chem. Theory Comput.* **2020**, *16*, 7239–7254.
52 Andersson, J.; Jarlebark, J.; Kk, S.; Schaefer, A.; Hailes, R.; Palasingh, C.; Santoso, B.; Vu, V.-T.; Huang, C.-J.; Westerlund, F. Polymer brushes on silica nanostructures prepared by aminopropylsilatrane click chemistry: superior antifouling and biofunctionality. *ACS Appl. Mater. Interfaces* **2023**, *15*, 10228–10239.
53 Klushin, L.; Skvortsov, A. Chain behavior in a polydisperse brush: Depression of critical fluctuations. *Macromolecules* **1992**, *25*, 3443–3448.
54 Bishop, M.; Kalos, M.; Frisch, H. Molecular dynamics of polymeric systems. *J. Chem. Phys.* **1979**, *70*, 1299–1304.

https://doi.org/10.1007/s10118-026-3605-x